Original Article | Open Access

Microbiome Research Reports

Zeng *et al. Microbiome Res Rep.* 2026;5:32 **DOI:**10.20517/mrr.2026.74

Mucin degradation by *Enterocloster* sp. M3 as an oncogenic mechanism in colorectal cancer

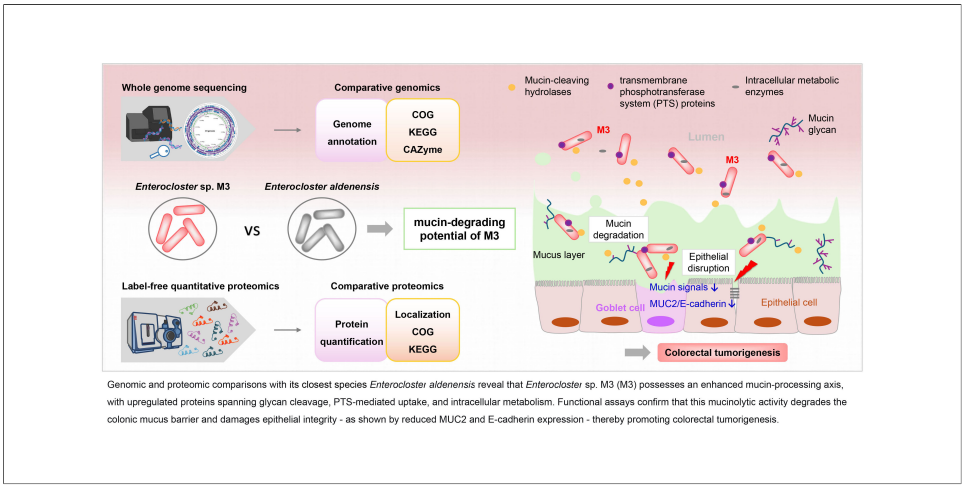
Yao Zeng[1], Silin Ye[1], Effie Yin Tung Lau[1], Ruoyu Hu[1], Jiawei Lu[1], Rui Zhang[1], Yanqing Huang[2], Shu Zheng[2], Jessie Qiaoyi Liang[1]

Keywords:
Enterocloster sp. M3, mucin degradation, colorectal cancer

Citation: Zeng Y, Ye S, Lau EYT, Hu R, Lu J, Zhang R, Huang Y, Zheng S, Liang JQ. Mucin degradation by *Enterocloster* sp. M3 as an oncogenic mechanism in colorectal cancer. *Microbiome Res Rep.* 2026;5:32. https://dx.doi.org/10.20517/mrr.2026.74

Received: 13 Aug 2026 **First Decision:** 9 Oct 2026 **Revised:** 16 Nov 2026 **Accepted:** 17 Nov 2026 **Published:** 27 Nov 2026

Academic Editor: Marco Ventura
Copy Editor: Shu-Yuan Duan
Production Editor: Shu-Yuan Duan



Genomic and proteomic comparisons with its closest species *Enterocloster aldenensis* reveal that *Enterocloster* sp. M3 (M3) possesses an enhanced mucin-processing axis, with upregulated proteins spanning glycan cleavage, PTS-mediated uptake, and intracellular metabolism. Functional assays confirm that this mucinolytic activity degrades the colonic mucus barrier and damages epithelial integrity - as shown by reduced MUC2 and E-cadherin expression - thereby promoting colorectal tumorigenesis.

Abstract

Background: *Enterocloster* sp. M3 (M3) has been implicated in colorectal cancer (CRC) through production of oncogenic metabolites, yet its interactions with colonic cells remain unclear. This study aimed to identify the functional role of M3 in CRC by genomic and proteomic comparison with its closest relative, *Enterocloster aldenensis* (*E. aldenensis*), followed by functional validation.

Methods: An integrated genomic and proteomic approach compared molecular features between M3 and *E. aldenensis*. Carbon source utilization assays compared the metabolic flexibility of M3 and *E. aldenensis*. *In vitro* mucin degradation and growth assays, alongside an *in vivo* mouse model, validated M3's mucin-degrading capacity and its impact on gut barrier function.

Results: Compared with *E. aldenensis*, genomics and proteomics revealed that M3 possesses enhanced metabolic potential for mucin utilization through a coordinated axis spanning extracellular glycan cleavage [e.g., glycoside hydrolases (GHs) /

Check for updates

[1]Department of Medicine and Therapeutics, Li Ka Shing Institute of Health Sciences, Centre for Gut Microbiota Research, The Chinese University of Hong Kong, Hong Kong, China; CUHK Shenzhen Research Institute, Shenzhen 518057, Guangdong, China.
[2]Second Affiliated Hospital, Zhejiang University College of Medicine, Hangzhou 310000, Zhejiang, China.

Correspondence to: Prof. Jessie Qiaoyi Liang, Department of Medicine and Therapeutics, Li Ka Shing Institute of Health Sciences, Centre for Gut Microbiota Research, The Chinese University of Hong Kong, Hong Kong 000000; CUHK Shenzhen Research Institute, Shenzhen 518057, Guangdong, China. E-mail: JessieQY@cuhk.edu.hk

mannosyl-glycoprotein endo-beta-N-acetylglucosaminidases (ENGases)] transmembrane phosphotransferase system (PTS)-mediated internalization, and intracellular metabolic processing [e.g., *N*-acetylglucosamine-6-phosphate (GlcNAc-6-P) deacetylase, fructose-bisphosphate aldolase, and L-fucose isomerase]. Phenotypic metabolic profiling demonstrated M3's versatile capacity to utilize diverse carbon and nitrogen sources, particularly mucin-related sugars. *In vitro* assays further showed that M3 exhibited accelerated mucinolytic activity and a marked growth advantage over *E. aldenensis* and *Escherichia coli* in mucin-supplemented minimal medium. Importantly, in *Apc*$^{min/+}$ mice, M3 significantly accelerated colorectal tumorigenesis by driving mucus barrier degradation, as evidenced by reduced colonic mucin signals and decreased mucin 2 (MUC2) and E-cadherin expression.

Conclusions: M3 possesses a highly efficient mucin-degrading genomic and proteomic repertoire that degrades the colonic mucus barrier and disrupts epithelial integrity, thereby accelerating colorectal tumorigenesis.

INTRODUCTION

Colorectal cancer (CRC) is a major global health concern closely associated with gut microbiota dysbiosis, characterized by enrichment of pathogenic bacteria and depletion of beneficial commensals. Previous studies have established the pro-tumorigenic roles of various pathogenic bacteria, including *Fusobacterium nucleatum*[1-3], polyketide synthase-harboring *Escherichia coli* (*E. coli*)[4,5], and enterotoxigenic *Bacteroides fragilis* (ETBF)[6-8]. These bacteria contribute to colorectal tumorigenesis by disrupting gut epithelial barrier integrity, promoting chronic inflammation, producing genotoxins, and modulating host immune responses. With the widespread application of metagenomic analyses, an increasing number of CRC-associated bacteria, including previously uncultured and unclassified taxa, are being identified. Elucidating the functional mechanisms of these bacteria is essential for a deeper understanding of the complex relationship between gut dysbiosis and CRC.

In our prior work, a 1,935-bp bacterial DNA marker, designated 'm3', was identified through metagenomic shotgun sequencing as a promising diagnostic marker for CRC and adenoma[9]. We subsequently isolated the m3-carrying bacterium from a patient with colonic adenoma and designated it *Enterocloster* sp. M3 (M3)[10]. M3 is phylogenetically close to *Enterocloster aldenensis* (*E. aldenensis*), as supported by 16S ribosomal DNA (16S rDNA) sequencing, matrix-assisted laser desorption ionization (MALDI) biotyping, and whole-genome sequencing demonstrating a high fastANI (average nucleotide identity) of 98.5% with moderate coverage for M3 (87.5%) and *E. aldenensis* (77.9%). However, M3 differs from the *E. aldenensis* type strain RMA 9741 in cell size and carbon source utilization profiles and, unlike other *E. aldenensis* strains, carries the m3 gene. Although these comprehensive phylogenetic analyses suggest their classification as different strains of the same species, we retain the designation *Enterocloster* sp. M3 to maintain continuity with our previous study and to highlight its unique phenotypic and pathogenic features[10]. We further demonstrated the pro-tumorigenic role of M3 in colorectal tumorigenesis *in vitro* and in mouse models, with significantly greater tumorigenic activity than *E. aldenensis*. Although we have revealed the first-reported bacterial production of the carcinogen styrene by M3, whether M3 possesses additional virulence features, particularly those involved in disrupting the host physical defense barriers, remains to be determined.

Excessive bacterial mucin degradation compromises the protective mucosal barrier, driving inflammation, infection, and CRC development[11-13]. In this study, we systematically characterized the genomic and proteomic profiles of M3 in comparison with *E. aldenensis* to identify its mucin-degrading potential, and we further evaluated its capacity to impair gut barrier function *in vitro* and *in vivo*.

MATERIALS AND METHODS

Bacterial strains and culture conditions

M3 was isolated in our previous study[10] and has been deposited at the China Center for Type Culture Collection (PB 2024022). *E. aldenensis* type strain RMA 9741 was purchased from German Collection of Microorganisms and Cell Cultures (DSMZ) (19262, Germany) and used for all downstream *in vitro* assays, *in vivo* animal trials, and proteomic profiling in comparison with M3. *E. coli* MG1655 [American Type Culture Collection (ATCC) 700926, Manassas, Virginia, USA], a non-pathogenic human intestinal bacterium, served as a bacterial control. All bacterial strains in this study were cultured in Columbia broth (C0971, Sigma-Aldrich, Schnelldorf, Germany) at 37 °C under anaerobic conditions.

Genome annotation, functional comparison, and carbohydrate-active enzyme analysis

Genome annotation was performed using Bakta v1.1.0 via Proksee, and the genomic features were visualized as a circular map using Map Builder v2.0.5[14,15]. Homologous regions along with specific marker locations were identified using BLAST v1.5.0. Functional annotations for predicted protein sequences were performed using the eggNOG-mapper v2.1.13 pipeline to extract the preferred gene names, Gene Ontology (GO) terms, KEGG Orthology (KO) identifiers, Kyoto Encyclopedia of Genes and Genomes (KEGG) pathways, and Clusters of Orthologous Groups (COG) categories[16]. carbohydrate-active enzymes (CAZymes) were annotated using the dbCAN online server based on predicted protein sequences, with HMMER (against dbCAN-HMM and dbCAN-sub databases) and DIAMOND (against the CAZy database)[17]. Only annotations supported by at least two of the three tools were retained as high-confidence CAZyme genes. For comparative genomic analyses, the genome sequence of *E. aldenensis* strain K25-0101-E9 was retrieved from public database and used for comparison with M3 because it is the reference genome of *E. aldenensis* with superior assembly quality, high contiguity, and no detectable ambiguous N bases. Functional comparisons between M3 and *E. aldenensis* were performed by comparing the counts of coding sequences assigned or unassigned to each functional category against the total predicted coding sequences of each genome. Two-sided Fisher's exact tests with Benjamini-Hochberg correction were applied to evaluate differences in the proportion of genes assigned to each functional category between the two genomes, with significance set at adjusted $P < 0.05$. All comparative analyses and visualizations were conducted using R v4.6.1.

Label-free quantitative proteomics

Bacterial pellets from two separate biological replicates per group were solubilized in Radioimmunoprecipitation assay (RIPA) buffer, disrupted, and centrifuged to isolate supernatants for bicinchoninic acid (BCA)-based protein quantification. Peptide mixtures were analyzed on a Q Exactive HFX Orbitrap mass spectrometer equipped with an EASY-nLC 1200 system (Thermo Fisher Scientific, Waltham, MA, USA). Because M3 is a newly isolated strain from our team and is phylogenetically closely related to *E. aldenensis*, raw MS data were processed using Proteome Discoverer software (version 2.4.0.305) with the Sequest HT search engine and searched against the *E. aldenensis* UniProt FASTA database (https://www.uniprot.org/taxonomy/358742; downloaded in November 2022) as a reference proteome for homology-based protein identification. A false discovery rate (FDR) ≤ 0.01 was applied for peptide-spectrum matches and peptides. Unique and Razor peptides were used for protein quantification and total peptide amount for normalization. Differential proteins were defined using a pre-specified fold-change threshold of ≥ 20 or ≤ 0.05. Given the limited number of biological replicates ($n = 2$ per group), this stringent threshold was adopted to focus the analysis on proteins exhibiting extreme changes, thereby reducing the likelihood that the reported candidates reflect technical noise rather than genuine biological differences. Proteins meeting this criterion should be regarded as exploratory candidates requiring independent experimental validation. An empirical Bayes moderated t-test was used to calculate raw *P* values to improve variance estimation given two biological replicates per group, followed by Benjamini-Hochberg correction. Candidates with fold-change (FC) ≥ 20 or ≤ 0.05 and FDR ≤ 0.05 were defined as differentially expressed. Differential proteins were

subjected to COG/ Eukaryotic Orthologous Groups (KOG) analysis, subcellular localization prediction via LocTree3 (v1.0.1), and pathway enrichment analysis using the KEGG database. KEGG pathway enrichment analysis was performed using a one-tailed Fisher's exact test based on 2 × 2 contingency tables to generate raw *P*-values. The background set was the above-mentioned *E. aldenensis* UniProt reference proteome (November 2022; $N = 10,703$). Multiple-testing correction was subsequently applied to the raw *P*-values using the Benjamini-Hochberg method. Pathways with a raw *P*-value < 0.05 were selected for visualization, while a Benjamini-Hochberg adjusted *P*-value (FDR) < 0.1 was applied as a more stringent threshold to control the false discovery rate for downstream biological interpretation.

Carbon source utilization assay

Bacterial suspensions (150 μL) at an optical density at 600 nm (OD_{600}) of 0.5 were inoculated into Biolog AN MicroPlate (Anaerobe Identification Test Panel, Biolog, Hayward, CA, USA) preloaded with diverse carbon substrates, together with a tetrazolium-based redox indicator, for metabolic analysis. Catabolism of usable carbon sources generates reducing equivalents, which reduce the tetrazolium dye to colored formazan proportional to respiratory activity. As a high-throughput phenotypic screening platform, each microplate simultaneously performs 95 discrete substrate utilization tests along with an internal negative control (water). Following anaerobic incubation at 37 °C for 22 h, the plate was monitored sequentially using the Biolog incubation and reading system. Data collection ceased when colorimetric signals stabilized with no further visible change, and only this stable endpoint readout was retained for analysis. Then the substrate utilization preferences were categorized into three levels by the built-in Biolog algorithm, based on the colorimetric intensity relative to the negative control baseline: positive (noticeable purple color, hereafter defined as "strongly preferred"), borderline (faint color, hereafter defined as "preferred"), and negative (almost identical in appearance to the negative control well). Three independent biological replicates were analyzed for each bacterium in this experiment.

Mucin degradation assay

Mucin is a glycoprotein with abundant glycan side chains. The capacity of strains to utilize mucin-derived carbon was assessed by measuring total soluble carbohydrate in bacterial supernatants using the anthrone assay as described before[18], with a modified chromogenic incubation temperature. A carbohydrate-free inorganic salt minimal medium, the basal minimal medium (PML4600, Coolaber, China), was used, supplemented with 0.5% (w/v) porcine gastric mucin (M1778, Sigma-Aldrich) as the sole carbohydrate source. Before inoculation, strains were pre-cultured anaerobically in Columbia broth overnight and washed once with sterile phosphate-buffered saline (PBS) to remove residual carbon from preculture medium. Washed cells were resuspended and inoculated at an initial OD_{600} of 0.02. Following anaerobic incubation for 24 h, cultures were centrifuged at 10,000 ×*g* for 10 min to remove particulate unreacted mucin and bacterial cells. The resulting bacterial supernatants were mixed with 0.1% anthrone reagent in concentrated sulfuric acid (1:3, v/v), in which soluble carbohydrates are acid-hydrolyzed and dehydrated to furfural derivatives that form a blue-green complex. The mixtures were then incubated for 20 min at room temperature protected from light, and the absorbance was measured at 620 nm. Data are expressed as relative fold change by normalizing the OD_{620} value of each sample to the mean OD_{620} value of the broth control. All measurements were performed in three independent biological replicates.

Bacterial growth in mucin-supplemented minimal medium

M3, *E. aldenensis*, and *E. coli* were cultured anaerobically at 37 °C in minimal medium supplemented with 0.5% (w/v) porcine gastric mucin as the sole carbon source. Bacterial pretreatment and inoculation were performed as described in Section **Mucin degradation assay**, with an initial OD_{600} of 0.02. The optical density of the cultures was measured at 600 nm at 0, 12, 24, and 36 h to assess bacterial growth in three independent biological replicates. Relative growth was calculated by dividing the OD_{600} value at each time point by the corresponding 0 h OD_{600} for each strain.

Alcian Blue-Periodic Acid Schiff and immunohistochemical analyses of colon tissues

All animal treatment and tissue collection were completed in our previously published study[10], from which formalin-fixed, paraffin-embedded colon tissues used in this study were obtained. The transgenic *Apc*$^{min/+}$ mouse model, characterized by spontaneous intestinal adenoma development, was used to evaluate the effects of bacterial intervention. Briefly, 45 six-week-old male *Apc*$^{min/+}$ C57BL/6J mice were randomly assigned to four groups. All mice were maintained on a standard chow diet and received daily oral gavage of 200 μL of bacterial suspension [containing 1 × 10^9 colony-forming unit (CFU) of M3, *E. aldenensis*, or *E. coli* MG1655] or an equal volume of PBS for 12 weeks. The group sizes were n = 12 for the M3, *E. coli* MG1655, and PBS groups, and n = 9 for the *E. aldenensis* group. All mice survived until the defined experimental endpoint (12 weeks of intervention) without meeting any pre-specified exclusion criteria (such as ≥ 20% weight loss). At the end of the experiment, mice were humanely euthanized by CO_2 inhalation, and colon tissues were harvested immediately for fixation. All animal experimental procedures were approved by the Animal Experimentation Ethics Committee of The Chinese University of Hong Kong (Approval Ref. No. 21-107-NSF).

All histological staining, imaging, and quantitative analyses reported in this study were newly performed on the archived tissue specimens. Specifically, archived paraffin blocks were newly sectioned, deparaffinized, rehydrated, and subjected to Alcian Blue-Periodic Acid Schiff (AB-PAS) (G1285, Solarbio, Beijing, China) staining to visualize mucins. For immunohistochemical (IHC), sections underwent antigen retrieval and blocking, followed by overnight incubation at 4 °C with primary antibodies against mucin 2 (MUC2) (27675-1-AP, Proteintech, Wuhan, China) and E-cadherin (3195S, CST, Danvers, MA, USA). The percentage of positive staining area was calculated as the area of positive signals divided by the total tissue area.

Statistical analysis

All values are presented as mean ± standard deviation (SD) or violin plots with median and quartiles where appropriate. Two groups were compared using unpaired t-test or Mann-Whitney U test. Multiple groups were compared using one-way analysis of variance (ANOVA) followed by Tukey's post hoc test. Bacterial growth curves were analyzed using two-way repeated-measures ANOVA with Tukey's multiple comparisons test. All statistical tests were performed using GraphPad Prism 9.4.1 (GraphPad Software Inc., San Diego, CA). Statistical significance was defined as a two-sided P-value of < 0.05.

RESULTS

Comparative genomic characterization reveals mucin-degrading potential of M3

As the closest relative of M3, *E. aldenensis* exhibited weaker pro-tumorigenic effects than M3[10]. We therefore conducted whole-genome comparison between M3 and *E. aldenensis* to identify unique genomic features of M3. Whole-genome sequencing yielded a 5.7-Mb M3 assembly that is gene-dense and maps largely to *E. aldenensis* genome [Figure 1A]. Comparative genomic analysis revealed that M3 and *E. aldenensis* share the majority of genes, GO terms, KO terms, and metabolic pathways, while each possesses a limited number of unique genes, GO terms, KO terms, and metabolic pathways [Figure 1B and Supplementary Table 1]. Nevertheless, COG functional classification revealed that M3 harbors an expanded genetic repertoire dedicated to carbohydrate transport and metabolism, providing a genomic basis for adaptation to dynamic nutrient environments in the gut [Figure 1C and Supplementary Table 2]. Notably, M3 possesses a greater number of genes assigned to the COG category [L] (replication, recombination and repair) that may be worth further investigation. We further analyzed the unique genes of M3 and *E. aldenensis* to elucidate the mechanisms underlying their functional differences. KEGG analysis showed that more of the M3-unique genes fell into carbohydrate metabolism pathways (e.g., amino sugar and nucleotide sugar metabolism, galactose metabolism, glycan degradation, glycolysis/gluconeogenesis, and starch and

sucrose metabolism) [Figure 1D and Supplementary Table 3], indicating a broader sugar-utilization profile and potential capacity for host mucin catabolism. CAZyme profiling revealed that M3 encodes more glycoside hydrolases potentially involved in mucin glycan hydrolysis, particularly in the glycoside hydrolases (GH) 3 (exclusive to M3), GH31, and GH38 families that contain enzymes with broad carbohydrate substrate ranges [Figure 1E and Supplementary Table 4]. Specifically, GH3 β-*N*-acetylhexosaminidases, GH31 α-galactosidases, and GH38 α-mannosidases participate in mucin glycan degradation[19-23]. Together, these genomic features position M3 as a potential mucin degrader capable of efficiently cleaving the complex host mucin scaffold.

Comparative proteomic analysis corroborates mucin-degrading potential of M3

Proteomic analysis identified 162 upregulated and 151 downregulated proteins in M3 compared with *E. aldenensis* [Figure 2A and Supplementary Table 5]. Subcellular localization prediction demonstrated a greater number of upregulated proteins in the inner membrane and periplasm of M3, suggesting potentially enhanced survival and adaptability to gut environmental changes [Figure 2B and Supplementary Table 5]. COG classification showed that these differentially expressed proteins were highly enriched in carbohydrate transport and metabolism, consistent with genomic predictions and confirming M3's active proteomic adaptation to environmental sugar utilization [Figure 2C]. Furthermore, KEGG pathway enrichment analysis of the differentially expressed proteins highlighted specific functional modules critical for host mucin utilization and carbohydrate processing, including fructose and mannose metabolism, phosphotransferase system (PTS), ATP-binding cassette (ABC) transporters, and amino sugar and nucleotide sugar metabolism [Figure 2D].

Convergent genomic and proteomic evidence identifies a mucin-degrading enzymatic repertoire in M3

To further validate the mucin-degrading potential of M3 at the molecular level, we examined the mucin degradation-related enzymes at both gene and protein levels. Comparative genomic analysis revealed that M3 harbors a greater complement of core processing genes encoding *N*-acetylglucosamine-6-phosphate deacetylase, fructose-bisphosphate aldolase, and L-fucose isomerase compared to *E. aldenensis* [Figure 3A and Supplementary Table 6]. Proteomic profiling further demonstrated markedly elevated levels of mucin-utilization proteins in M3 compared with *E. aldenensis* [Figure 3B and Supplementary Table 7]. Both genomic and proteomic data converge on an expanded repertoire of mucin-cleaving hydrolases (e.g., GH3/18/38, ENGases) and an enriched PTS for sugar internalization and transport. These findings collectively demonstrate that M3 possesses more metabolic enzymes for host mucin utilization compared to *E. aldenensis*, supporting a superior capacity of M3 for host mucin catabolism.

M3 exhibits broad metabolic versatility and superior mucin-utilizing capacity

Phenotypic metabolic profiling by Biolog analysis revealed that M3 and *E. aldenensis* differ markedly in carbon and nitrogen source utilization under identical culture conditions [Figure 4A]. Analysis of strongly preferred and preferred substrates indicated that M3 is a metabolic generalist with superior carbon source utilization and complex nitrogen acquisition strategies. M3 also possesses specific metabolic traits, including D-lactic acid methyl ester utilization, mucin degradation potential, and the potential to decompose organic matter [Table 1]. Its ability to utilize N-acetyl-D-glucosamine (a component of mucin and chitin), L-fucose (a key mucin sugar), amino acids, and nucleosides is consistent with features of bacteria that have evolved to thrive in the gut environment. To further evaluate the functional relevance of this metabolic versatility, we compared the mucin utilization and growth of M3 and *E. aldenensis* in minimal medium containing porcine gastric mucin as the sole carbon source, alongside *E. coli* and broth controls. Soluble carbohydrate levels in M3 cultures at 24 h were significantly higher than those in *E. aldenensis*, *E. coli*, and broth controls, indicating highly efficient cleavage of mucin glycans by M3 [Figure 4B]. Consistent with its superior

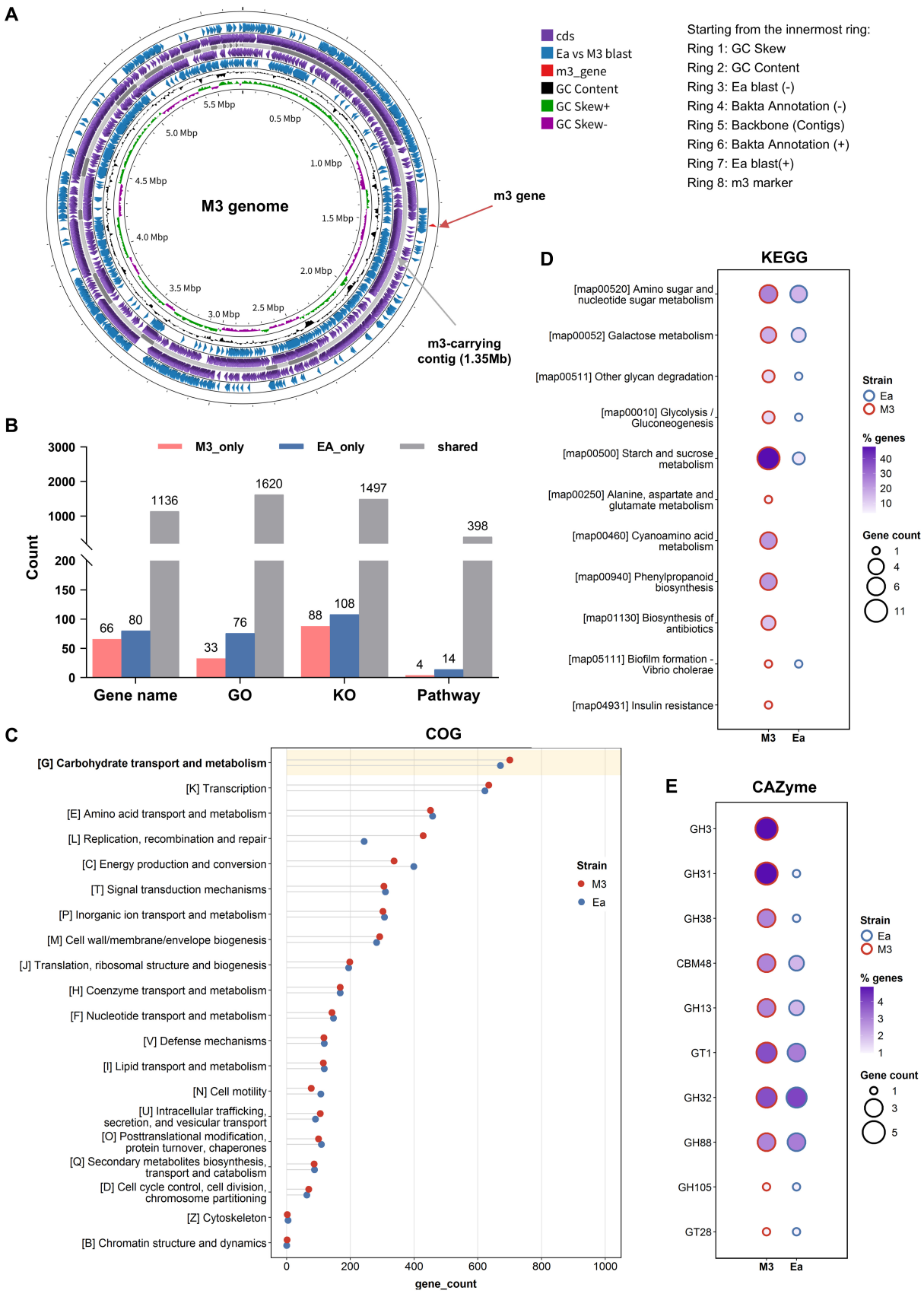


Figure 1. Comparative analysis of the M3 genome. (A) Circos plot providing an overview of the M3 genome, highlighting its structural features, functional annotations, and comparative genomics relative to the reference genome of *E. aldenensis* (Ea; strain K25-0101-E9). The eight concentric rings display distinct genomic data, as labeled. Rings 3 and 7 show BLAST-based comparisons between the M3 and Ea genomes, with continuous segments indicating significant regions of synteny. Each backbone in Ring 5 represents a contig, with the one carrying the m3 marker denoted. cds, coding sequences; (B) Genome feature comparison between M3 and Ea. The numbers of shared and unique genes, GO terms, KO terms, and pathways are shown; (C) COG functional classification. Gene counts for carbohydrate transport

and metabolism are higher in M3 than in Ea, suggesting that M3 is better adapted to utilize specific sugars; (D) KEGG pathways overrepresented in M3 relative to Ea. Compared with Ea, M3 exhibits higher gene representation in multiple carbon metabolism pathways, including amino sugar and nucleotide sugar metabolism, galactose metabolism, other glycan degradation, glycolysis/gluconeogenesis, and starch and sucrose metabolism; (E) CAZyme profiling shows that M3 contains a higher abundance and broader diversity of mucin-degrading glycoside hydrolases than Ea, particularly in GH3, GH31, and GH38 families. GC: guanine-cytosine; EA: *E. aldenensis*; M3: *Enterocloster* sp. M3; KEGG: Kyoto Encyclopedia of Genes and Genomes; GO: Gene Ontology; KO: KEGG Orthology; CAZyme: carbohydrate-active enzyme; COG: Clusters of Orthologous Groups.

mucinolytic efficiency, M3 exhibited significantly greater growth than *E. aldenensis* and *E. coli* over 36 h in the same medium [Figure 4C].

M3 drives excessive colonic mucus degradation and disrupts epithelial barrier integrity in vivo

To evaluate the role of M3 *in vivo*, AB-PAS and IHC analyses were newly performed on archived colon tissues from our previously established *Apc*$^{min/+}$ mouse cohort. *Apc*$^{min/+}$ mice were orally gavaged with M3, *E. aldenensis*, non-pathogenic *E. coli*, or PBS for 12 weeks [Figure 5A]. M3 administration significantly accelerated colorectal tumorigenesis, inducing a markedly higher colonic tumor burden compared with other groups[10]. AB-PAS staining of non-tumor colon tissues revealed the lowest mucin-positive signals in the M3 group, confirming excessive mucus degradation by M3 *in vivo* [Figure 5B]. IHC analysis further demonstrated that the levels of the colonic mucin constituent MUC2 and the epithelial barrier marker E-cadherin were significantly reduced in the M3-treated group compared with other groups [Figure 5C]. These findings collectively suggest that M3 promotes colorectal tumorigenesis, at least in part, by driving mucus barrier degradation and disrupting epithelial integrity.

DISCUSSION

In this study, through systematic comparison of genomic and proteomic profiles, we elucidated unique metabolic and virulence features distinguishing the newly isolated *Enterocloster* sp. M3 from its closest relative, *E. aldenensis*. M3 emerges as a metabolically versatile anaerobe that is exceptionally well-adapted to the glycan-rich and highly competitive gut environment. In particular, M3 exhibits mucin-degrading potential that represents a recognized mechanism by which gut microbiota may contribute to colorectal carcinogenesis. Mechanistically, M3 outcompetes *E. aldenensis* through a highly efficient axis encompassing extracellular glycan cleavage, enhanced transmembrane PTS-mediated internalization, and more copies and elevated expression of genes encoding intracellular metabolic enzymes, including L-fucose isomerase, GlcNAc-6-P deacetylase, and fructose-bisphosphate aldolase. Although genomic copy numbers do not always strictly correspond to *in vitro* protein abundances, the profiles of these mucin-degrading enzymes were largely concordant across both datasets. The minor decoupling observed for a small subset of targets might be due to the difference in regulatory elements at DNA level or post-transcriptional regulation. Consistently, phenotypic and growth analyses confirmed that M3 utilizes a broader spectrum of mucin-related substrates, hydrolyzes mucin at an accelerated rate, and grows significantly better in minimal medium supplemented with mucin as the only carbon source, collectively supporting its potent mucin-degrading and utilization activity.

Previous reports indicated that colonic mucins in mice are robustly fucosylated, with L-fucose accumulation on glycans markedly exceeding that in small intestine[24-26]. In humans, in chronic pathologies such as ulcerative colitis, aberrant upregulation of the glycosyltransferase responsible for catalyzing fucosylation has been specifically observed in the distal colon[27], indicating fucose-decorated glycans could be pathologically enriched in the inflamed colon. Crucially, our study revealed that M3 expresses high levels of L-fucose isomerase. This key enzyme likely enables the bacterium to efficiently utilize host-derived fucose as a metabolic substrate. Notably, as colonic fucosylation primarily occurs on MUC2[26], the significant decrease in MUC2 expression levels observed in the M3-treated mice implies that M3 may actively utilize and

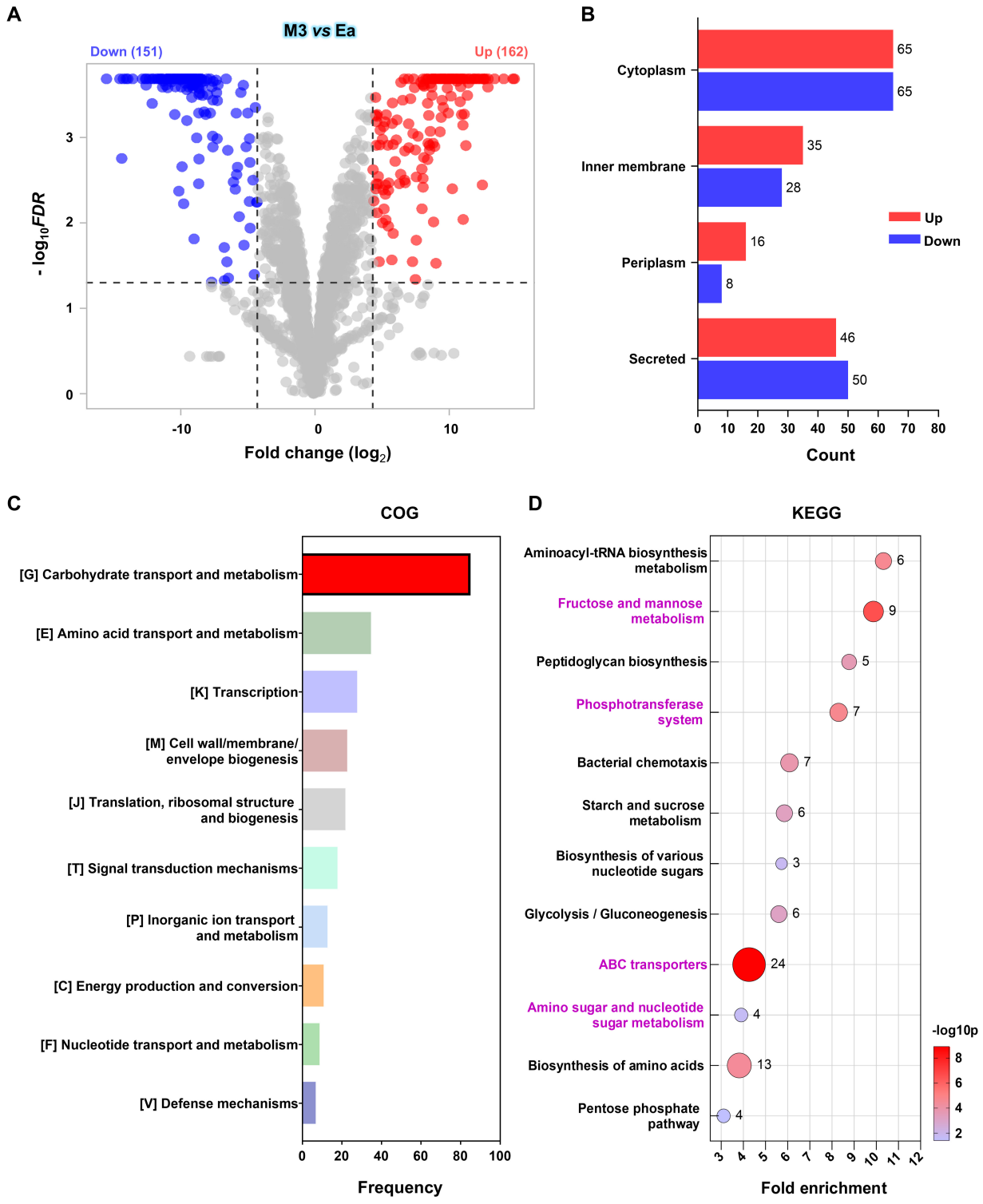


Figure 2. Proteomic comparison between M3 and *E. aldenensis*. (A) Volcano plot showing the differential proteins in M3 compared to Ea. Proteins were considered differentially expressed using cut-off thresholds of fold change ≥ 20 or ≤ 0.05 and FDR ≤ 0.05; (B) More proteins located in the inner membrane and periplasm are upregulated in M3, potentially enhancing its gut survival and adaptability; (C) COG functional classification of the differential proteins between M3 and Ea, with the largest fraction assigned to carbohydrate transport and metabolism; (D) KEGG pathway enrichment analysis of the differential proteins, highlighting pathways involved in host mucin utilization and carbohydrate processing, including fructose and mannose metabolism, PTS, ABC transporters, and amino sugar and nucleotide sugar metabolism. Pathways with a raw *P*-value < 0.05 were selected for visualization (all FDR <0.1). The color gradient represents the -$\log_{10}$(raw *P*-value). M3: *Enterocloster* sp. M3; Ea: *Enterocloster aldenensis*; tRNA: transfer RNA; FDR: false discovery rate; COG: Clusters of Orthologous Groups; KEGG: Kyoto Encyclopedia of Genes and Genomes; PTS: phosphotransferase system; ABC: ATP-binding cassette.

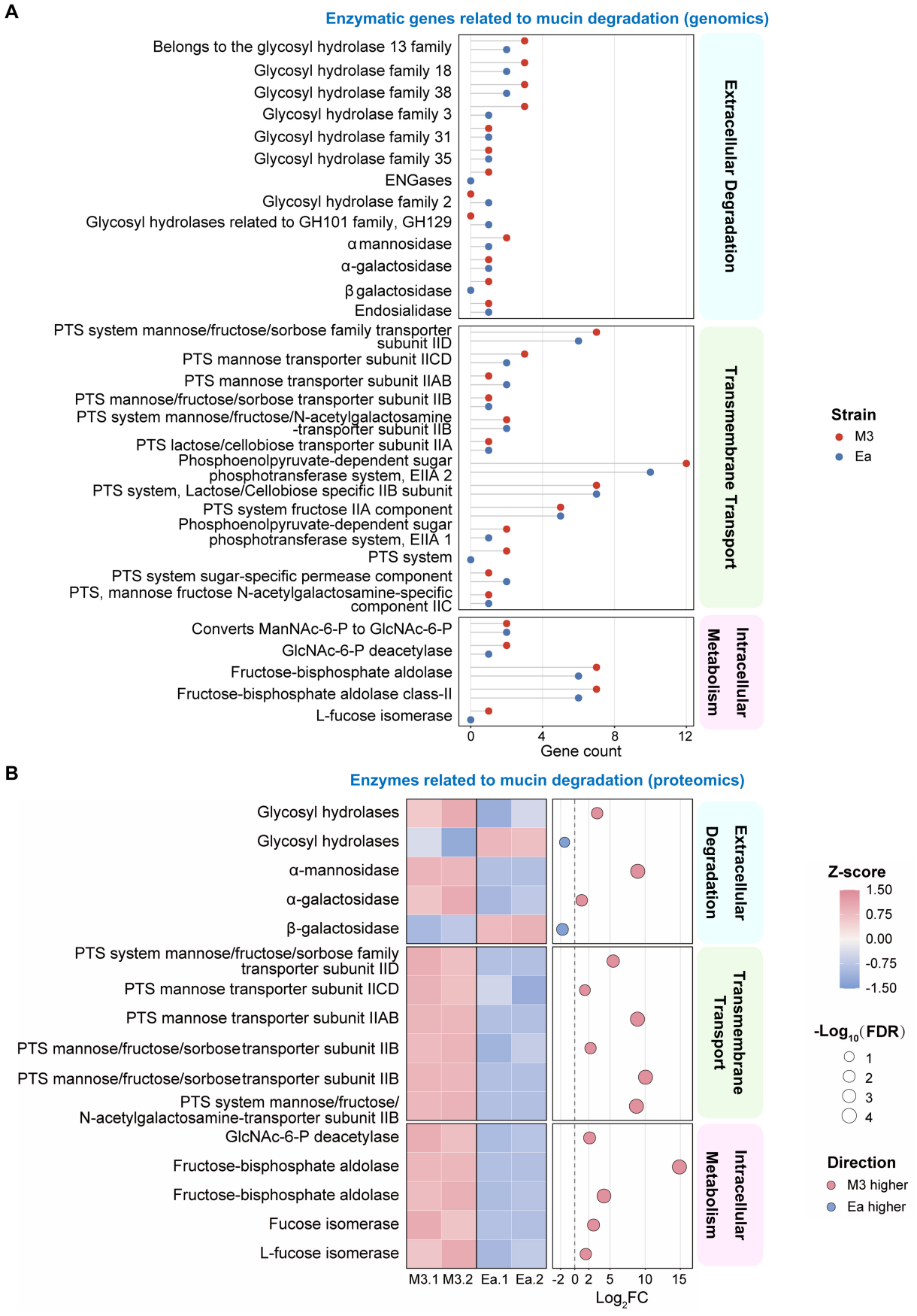


Figure 3. Genomic and proteomic profiling of mucin-degradation-associated genes and proteins in M3 and *E. aldenensis*. (A) Genomic analysis showing increased gene counts in M3 across mucin degradation, transport, and metabolism processes; (B) Proteomic heatmap confirming higher levels of the corresponding proteins in M3 than in Ea. ENGases: Mannosyl-glycoprotein endo-beta-N-acetylglucosaminidases; PTS: phosphotransferase system; ManNAc-6-P: *N*-acetylmannosamine-6-phosphate; GlcNAc-6-P: *N*-

acetylglucosamine-6-phosphate; FC: fold change; FDR: false discovery rate; M3: *Enterocloster* sp. M3; Ea: *Enterocloster aldenensis*.

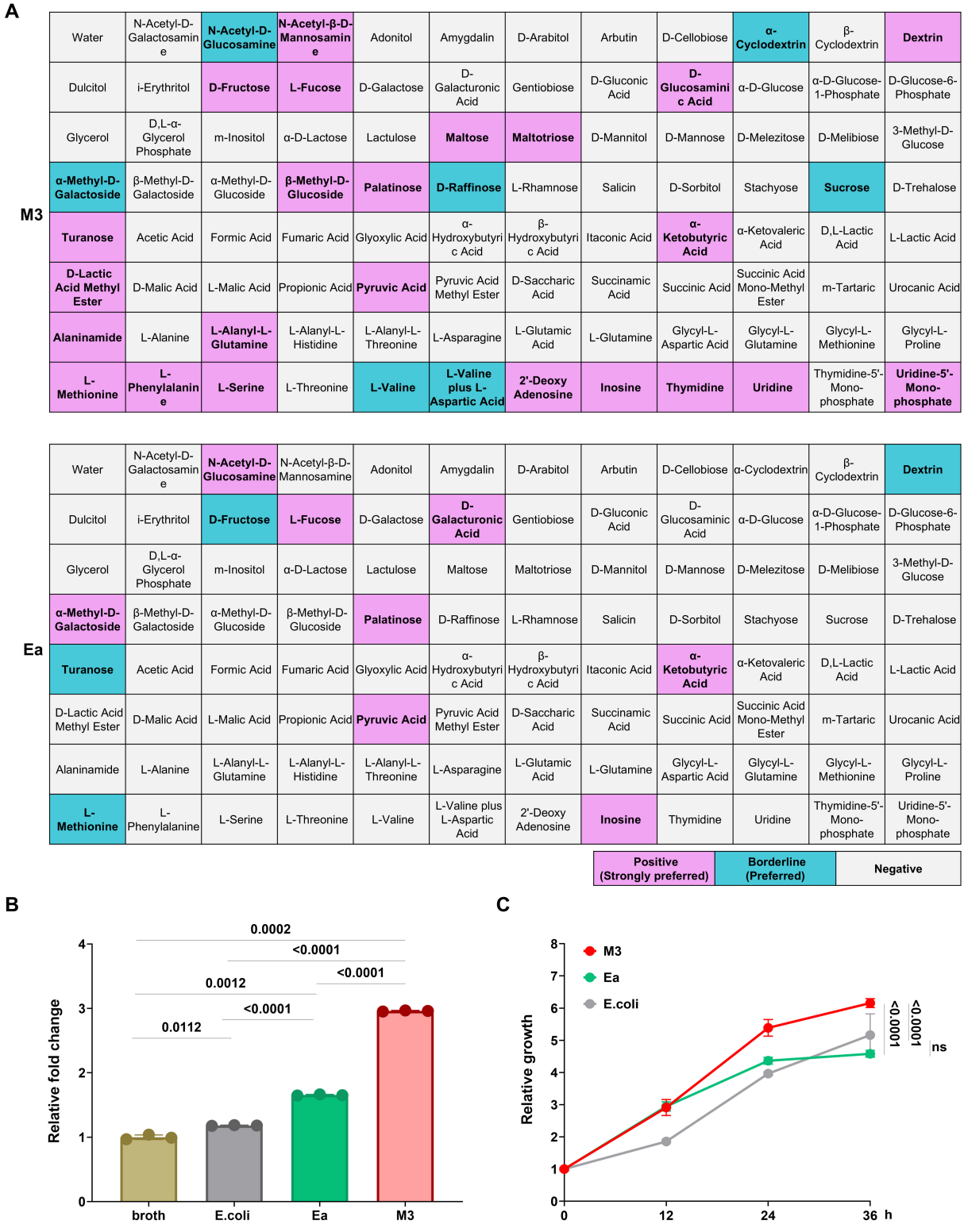


Figure 4. M3 exhibits superior utilization of mucin-derived carbon substrates compared to *E. aldenensis*. (A) Comparison of carbon and nitrogen source utilization, indicating the substrate preferences of M3 versus Ea; (B) Relative fold change in soluble carbohydrate in culture supernatants, as measured by the anthrone assay and normalized to the mean value of the broth control; (C) Growth curves of bacteria cultured in minimal medium with porcine gastric mucin as the sole carbon source. Data are presented as mean ± SD. Data were compared among groups using one-way ANOVA (Tukey's post hoc test) (B) or two-way repeated-measures ANOVA with Tukey's multiple comparisons test (C). M3: *Enterocloster* sp. M3; Ea: *Enterocloster aldenensis*; ANOVA: analysis of variance; SD: standard deviation; *E. coli*: *Escherichia coli*.

Table 1. Profile of strongly preferred and preferred carbon and nitrogen sources utilized by M3

Category	Function/metabolism	Strongly preferred / preferred
Exceptional capability in carbon source utilization	Complex polymer degradation	α-cyclodextrin
		Dextrin
		N-acetyl-d-glucosamine
	Diverse sugar utilization	N-acetyl-β-d-mannosamine
		D-fructose
		Sucrose
		Maltose
		Palatinose
		Turanose
		D-raffinose
		Maltotriose
		α-methyl-d-galactoside
		β-methyl-d-glucoside
	Organic acid metabolism	Pyruvic acid
		α-ketobutyric acid
		D-glucosaminic acid
Sophisticated nitrogen acquisition strategies	Amino acid metabolism	L-Serine
		L-valine
		L-methionine
		L-phenylalanine
	Peptide utilization	L-valine plus l-aspartic acid
		Alaninamide
		L-alanyl-l-glutamine
	nucleoside/Nucleotide scavenging	Inosine
		Uridine
		Thymidine
		2′-deoxyadenosine
		Uridine-5′-monophosphate
Specific Metabolic Traits	D-lactic acid methyl ester utilization	D-lactic acid methyl ester
	Mucin degradation potential	N-acetyl-d-glucosamine
		L-fucose
		Dextrin
	Potential in decomposing organic matter	α-cyclodextrin
		N-acetyl-d-glucosamine

Only utilized substrates are listed, classified as "strongly preferred" or "preferred", which correspond to "positive" and "borderline" readouts respectively in the Biolog AN MicroPlate assay.

dismantle the fucosylated mucin matrix. These findings confer a potential colonization advantage of M3 within fucosylated niches and its contribution to compromising mucosal barrier integrity and accelerating tumorigenesis. However, studies in clinical cohorts are required to verify M3's colonic spatial enrichment and to validate its potential as a site-specific diagnostic biomarker.

Intestinal mucus degradation by gut bacteria is a double-edged sword: it can be both beneficial and harmful, depending on the context and balance within the gut environment. On one hand, controlled mucus

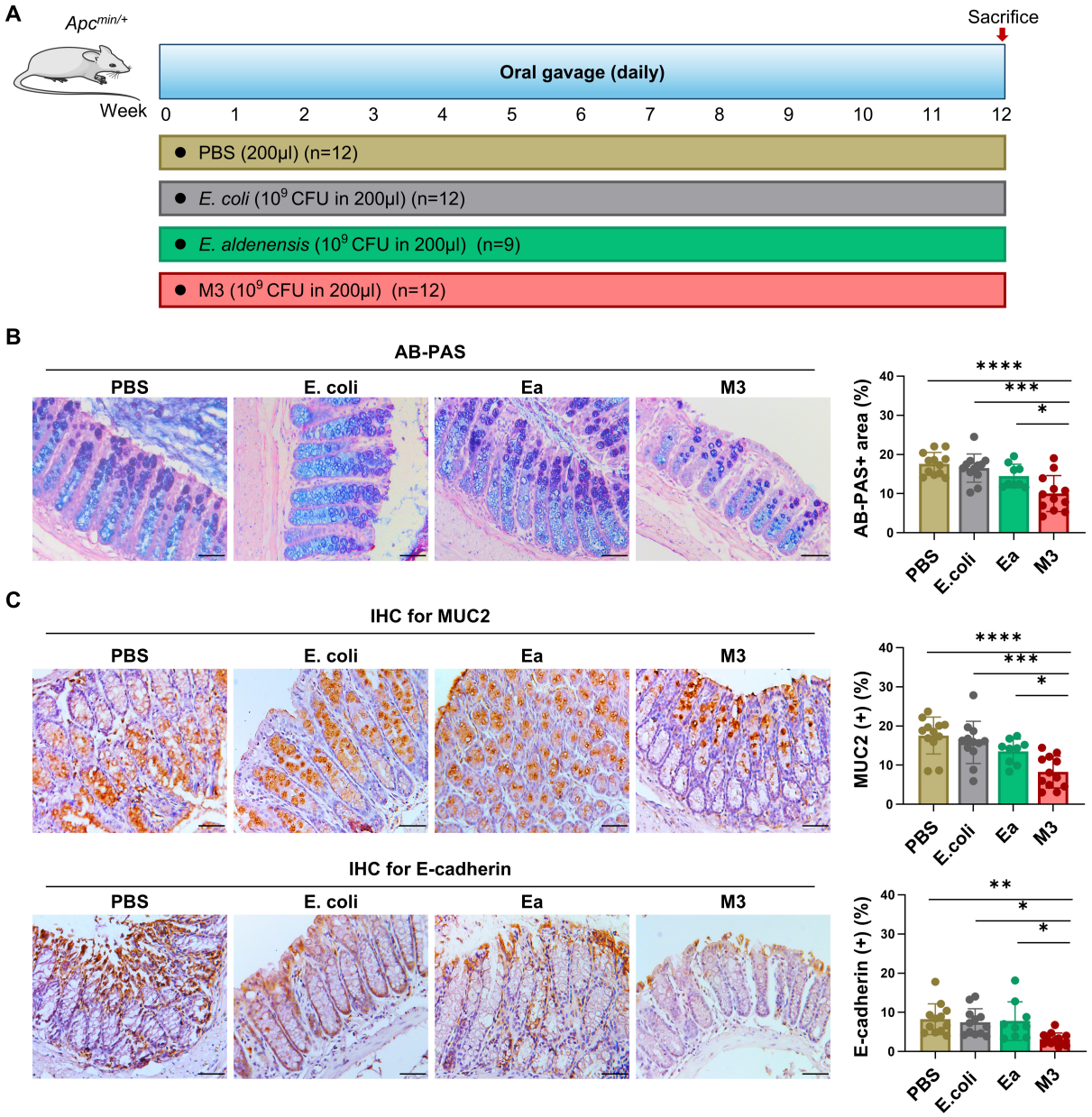


Figure 5. *In vivo* evaluation of mucin degradation and mucosal barrier disruption by M3. (A) Newly created schematic summarizing the prior animal experimental design from which the archived colon tissues were sourced; (B) AB-PAS staining of colon tissues to quantify the relative area percentage of mucin-positive signals; (C) IHC staining showing that the levels of the colonic mucin constituent MUC2 and the epithelial barrier marker E-cadherin are significantly decreased in the M3-treated group relative to the other groups. Data are presented as mean ± SD. Figure 5B and C, scale bars = 50 μm. *$P < 0.05$, ** $P < 0.01$, *** $P < 0.001$, **** $P < 0.0001$ by one-way ANOVA (Tukey's post hoc test). M3: *Enterocloster* sp. M3; Ea: *Enterocloster aldenensis*; AB-PAS: Alcian Blue-Periodic Acid Schiff; IHC: immunohistochemical; PBS: phosphate-buffered saline; CFU: colony-forming unit; MUC2: mucin 2; SD: standard deviation; ANOVA: analysis of variance; *E. coli*: *Escherichia coli*.

degradation enables commensal bacteria to establish a niche and outcompete pathogens, contributing to colonization resistance[28,29]. On the other hand, excessive degradation can compromise the mucus barrier, allowing bacteria to directly contact the intestinal epithelium and trigger inflammatory responses[11,30,31]. Moreover, bacterial degradation of the mucus layer also exposes epithelial cells to bacterial metabolites, such as lipopolysaccharides and genotoxins, thereby fostering a pro-inflammatory microenvironment conducive to cellular damage and DNA mutations. Furthermore, mucus degradation alters oxygen distribution in the gut, generating a more aerobic microenvironment at the epithelial surface that favors expansion of facultative

anaerobes such as *Fusobacterium nucleatum*, which in turn promotes CRC progression. Several mucin-degrading bacteria have been implicated in CRC, including *Akkermansia muciniphila* and ETBF. Although *Akkermansia muciniphila* is regarded as a next-generation beneficial microorganism[32], it is enriched in CRC and has been implicated in promoting colorectal tumorigenesis[12,33], with pro-tumorigenic effects largely attributed to excessive mucin degradation and disruption of the gut barrier[34]. Similarly, impairment of the intestinal mucus layer has been shown to exacerbate the pathogenicity of ETBF[35]. We previously established the pro-tumorigenic role of M3 through the production of carcinogenic metabolites[10]. Here, we uncover an additional pathogenic mechanism involving excessive host mucin degradation with its broad metabolic versatility and its progressive enrichment during the adenoma-carcinoma sequence. Our multi-omic comparisons, *in vitro*, and *in vivo* findings demonstrate M3's superior ability to degrade mucins and utilize mucin-derived carbon compared to *E. aldenensis*, likely contributing to its elevated pro-tumorigenic potential relative to *E. aldenensis*. This M3-mediated mucin foraging disrupts the mucosal barrier, constituting a distinct pathogenic trait that complements its established chemical oncogenic activity and underscores the multifaceted nature of M3-mediated colorectal tumorigenesis. Although our current dataset cannot fully separate the relative contributions of mucin degradation from these parallel oncogenic pathways, we hypothesize that mucin degradation may act as an upstream initiating event. Future studies using enzyme-deficient M3 mutants will be required to disentangle these parallel mechanisms.

There are some limitations in our study. For proteomic analysis, we searched against the *E. aldenensis* database only, which may miss M3-specific or divergent enzymes. However, this strategy would theoretically underestimate the full metabolic capacity of M3 as well as its mucin-degrading capacity relative to *E. aldenensis*. Nevertheless, the significant upregulation of shared mucin-associated proteins supports the prominent mucin-degradative profile of M3 under identical culture conditions. Although the *Apc*$^{min/+}$ model reveals the pathogenic role of M3 in mucus degradation and tumorigenesis *in vivo*, it does not fully recapitulate the spatial mucin glycosylation gradients and complex microbiota of the human colon. Thus, caution is warranted when extrapolating these animal model findings to human CRC. Future studies using clinical cohorts are essential to translate these mechanistic insights into human pathophysiology. Comparative proteomic analysis included only two biological replicates per group and is therefore considered exploratory screening. Nevertheless, M3 and *E. aldenensis* exhibit markedly distinct pathogenic and mucin-degradative capacities, which were validated in subsequent *in vitro* and *in vivo* assays.

This study indicates that the CRC marker-carrying bacterium M3 possesses a superior capacity to degrade host mucin, driving excessive destruction of the protective colonic mucus barrier and thereby accelerating colorectal tumorigenesis.

DECLARATIONS

Authors' contributions

Writing - original draft: Zeng Y
Visualization: Zeng Y, Ye S, Hu R
Investigation: Zeng Y, Ye S, Lau EYT, Lu J, Zhang R, Huang Y, Zheng S, Liang JQ
Formal analysis: Zeng Y, Ye S, Liang JQ
Data curation: Zeng Y, Ye S, Lau EYT, Liang JQ
Genome annotation: Ye S
Resources: Zheng S, Liang JQ
Project administration: Zheng S, Liang JQ
Conceptualization: Liang JQ
Supervision: Liang JQ
Funding acquisition: Liang JQ
Writing - review & editing: Liang JQ

Availability of data and materials

The M3 isolate has been deposited at the China Center for Type Culture Collection (CCTCC; http://cctcc.whu.edu.cn/index.php) under accession number CCTCC PB 2024022. This whole genome of M3 has been deposited at DDBJ/ENA/GenBank under accession JBKHUJ000000000, with the version described in this paper being JBKHUJ010000000. Proteomic data generated in this study are publicly available in iProX (https://www.iprox.cn/), a member of ProteomeXchange, under accession number PXD064607. Other unique/stable reagents in this study are available from the lead contact with a completed material transfer agreement.

AI and AI-assisted tools statement

Not applicable.

Financial support and sponsorship

This project was supported by the National Natural Science Foundation of China (grant 82372587).

Conflicts of interest

The authors declare no conflict of interest.

Ethical approval and consent to participate

All animal procedures were approved by the Animal Ethics Committee of The Chinese University of Hong Kong (AEEC ref# 21-107-NSF).

Consent for publication

Not applicable.

Copyright

© The Author(s) 2026.

Supplementary Materials

Supplementary Materials

REFERENCES

1. Kostic AD, Chun E, Robertson L, et al. Fusobacterium nucleatum potentiates intestinal tumorigenesis and modulates the tumor-immune microenvironment. *Cell Host Microbe.* 2013;14:207-15. DOI PubMed PMC
2. Wang Z, Li B, Bao L, et al. Fusobacterium nucleatum aggravates intestinal barrier impairment and colitis through IL-8 induced neutrophil chemotaxis by activating epithelial cells. *J Inflamm Res.* 2024;17:8407-20. DOI PubMed PMC
3. Rubinstein MR, Wang X, Liu W, Hao Y, Cai G, Han YW. *Fusobacterium nucleatum* promotes colorectal carcinogenesis by modulating E-cadherin/β-catenin signaling via its FadA adhesin. *Cell Host Microbe.* 2013;14:195-206. DOI PubMed PMC
4. Nasrollahian S, Halaji M, Bakeshloo PH, Abdullah M, Chang YF. Role of pks + Escherichia coli in colorectal cancer: mechanisms, clinical evidence, and therapeutic perspective. *Infect Genet Evol.* 2026;144:106003. DOI PubMed
5. Lv C, Abdullah M, Chen W, et al. Genomic characterization of *Escherichia coli* harbor a polyketide synthase (pks) island associated with colorectal cancer (CRC) development. *bioRxiv.* 2024. DOI PubMed PMC
6. Wu S, Rhee KJ, Albesiano E, et al. A human colonic commensal promotes colon tumorigenesis via activation of T helper type 17 T cell responses. *Nat Med.* 2009;15:1016-22. DOI PubMed PMC
7. Chen J, An Y, Tong A, et al. Bacteroides fragilis toxin promotes gall bladder cancer in mice. *Nat Microbiol.* 2026;11:2601-18. DOI PubMed PMC
8. Cao Y, Wang Z, Yan Y, et al. Enterotoxigenic *Bacteroides fragilis* promotes intestinal inflammation and malignancy by inhibiting exosome-packaged miR-149-3p. *Gastroenterology.* 2021;161:1552-1566.e12. DOI
9. Liang JQ, Li T, Nakatsu G, et al. A novel faecal *Lachnoclostridium* marker for the non-invasive diagnosis of colorectal adenoma and cancer. *Gut.* 2020;69:1248-57. DOI PubMed PMC
10. Zeng Y, Huang Y, Ye S, et al. Novel bacterium *Enterocloster* sp. M3 promotes colorectal tumorigenesis via the production of the carcinogen styrene. *Gut Microbes.* 2026;18:2630481. DOI PubMed PMC
11. Desai MS, Seekatz AM, Koropatkin NM, et al. A dietary fiber-deprived gut microbiota degrades the colonic mucus barrier and enhances pathogen susceptibility. *Cell.* 2016;167:1339-1353.e21. DOI PubMed PMC

12. Qu S, Zheng Y, Huang Y, et al. Excessive consumption of mucin by over-colonized Akkermansia muciniphila promotes intestinal barrier damage during malignant intestinal environment. *Front Microbiol.* 2023;14:1111911. DOI PubMed PMC
13. Chen Y, Xu Y, Li X, et al. The role of gut microbiota and mucin barrier in the pathogenesis of colorectal cancer. *Curr Issues Mol Biol.* 2025;48:16. DOI PubMed PMC
14. Grant JR, Enns E, Marinier E, et al. Proksee: in-depth characterization and visualization of bacterial genomes. *Nucleic Acids Res.* 2023;51:W484-92. DOI PubMed PMC
15. Schwengers O, Jelonek L, Dieckmann MA, Beyvers S, Blom J, Goesmann A. Bakta: rapid and standardized annotation of bacterial genomes via alignment-free sequence identification. *Microb Genom.* 2021;7:000685. DOI PubMed PMC
16. Cantalapiedra CP, Hernández-Plaza A, Letunic I, Bork P, Huerta-Cepas J. eggNOG-mapper v2: functional annotation, orthology assignments, and domain prediction at the metagenomic scale. *Mol Biol Evol.* 2021;38:5825-9. DOI PubMed PMC
17. Zheng J, Ge Q, Yan Y, Zhang X, Huang L, Yin Y. dbCAN3: automated carbohydrate-active enzyme and substrate annotation. *Nucleic Acids Res.* 2023;51:W115-21. DOI PubMed PMC
18. Pan M, Barua N, Ip M. Mucin-degrading gut commensals isolated from healthy faecal donor suppress intestinal epithelial inflammation and regulate tight junction barrier function. *Front Immunol.* 2022;13:1021094. DOI PubMed PMC
19. Xiao M, Zhang C, Duan H, et al. Cross-feeding of bifidobacteria promotes intestinal homeostasis: a lifelong perspective on the host health. *NPJ Biofilms Microbiomes.* 2024;10:47. DOI PubMed PMC
20. Qian K, Yang W, Chen X, Wang Y, Zhang M, Wang M. Functional and structural characterization of a GH3 β-N-acetylhexosaminidase from *Akkermansia muciniphila* involved in mucin degradation. *Biochem Biophys Res Commun.* 2022;589:186-91. DOI
21. Miyazaki T, Ishizaki Y, Ichikawa M, Nishikawa A, Tonozuka T. Structural and biochemical characterization of novel bacterial α-galactosidases belonging to glycoside hydrolase family 31. *Biochem J.* 2015;469:145-58. DOI PubMed
22. Cobucci-Ponzano B, Conte F, Strazzulli A, et al. The molecular characterization of a novel GH38 α-mannosidase from the crenarchaeon *Sulfolobus solfataricus* revealed its ability in de-mannosylating glycoproteins. *Biochimie.* 2010;92:1895-907. DOI
23. Bakshani CR, Ojuri TO, Pilgaard B, et al. Carbohydrate-active enzymes from Akkermansia muciniphila break down mucin O-glycans to completion. *Nat Microbiol.* 2025;10:585-98. DOI PubMed PMC
24. Schneider M, Al-Shareffi E, Haltiwanger RS. Biological functions of fucose in mammals. *Glycobiology.* 2017;27:601-18. DOI PubMed PMC
25. Larsson JM, Thomsson KA, Rodríguez-Piñeiro AM, Karlsson H, Hansson GC. Studies of mucus in mouse stomach, small intestine, and colon. III. Gastrointestinal Muc5ac and Muc2 mucin O-glycan patterns reveal a regiospecific distribution. *Am J Physiol Gastrointest Liver Physiol.* 2013;305:G357-63. DOI PubMed PMC
26. Li Y, Pan J, Liu H, Liu C. Intestinal mucin glycosylation: structural regulation, homeostasis maintenance and disease association. *Biomolecules.* 2025;15:1552. DOI PubMed PMC
27. Cantero-Recasens G, Burballa C, Ohkawa Y, et al.; IBD Character Consortium. The ulcerative colitis-associated gene FUT8 regulates the quantity and quality of secreted mucins. *Proc Natl Acad Sci U S A.* 2022;119:e2205277119. DOI PubMed PMC
28. Ronkainen A, Khan I, Satokari R. Pathogen exclusion from intestinal mucus and antimicrobial susceptibility of *Bifidobacterium* spp. strains from fecal donors. *Microbiome Res Rep.* 2025;4:5. DOI PubMed PMC
29. Collado MC, Gueimonde M, Hernández M, Sanz Y, Salminen S. Adhesion of selected *Bifidobacterium* strains to human intestinal mucus and the role of adhesion in enteropathogen exclusion. *J Food Prot.* 2005;68:2672-8. DOI PubMed
30. Kordahi MC, Daniel N, Gewirtz AT, Chassaing B. Mucus-penetrating microbiota drive chronic low-grade intestinal inflammation and metabolic dysregulation. *Gut Microbes.* 2025;17:2455790. DOI PubMed PMC
31. Tingler AM, Engevik MA. Breaking down barriers: is intestinal mucus degradation by *Akkermansia muciniphila* beneficial or harmful? *Infect Immun.* 2025;93:e0050324. DOI PubMed PMC
32. Cani PD, Depommier C, Derrien M, Everard A, de Vos WM. *Akkermansia muciniphila*: paradigm for next-generation beneficial microorganisms. *Nat Rev Gastroenterol Hepatol.* 2022;19:625-37. DOI PubMed
33. Osman MA, Neoh HM, Ab Mutalib NS, et al. *Parvimonas micra*, *Peptostreptococcus stomatis*, *Fusobacterium nucleatum* and *Akkermansia muciniphila* as a four-bacteria biomarker panel of colorectal cancer. *Sci Rep.* 2021;11:2925. DOI PubMed PMC
34. Soheilipour M, Noursina A, Nekookhoo M, et al. The pathobiont role of *Akkermansia muciniphila* in colorectal cancer: a systematic review. *BMC Gastroenterol.* 2025;25:702. DOI PubMed PMC
35. Hecht AL, Casterline BW, Choi VM, Bubeck Wardenburg J. A two-component system regulates *Bacteroides fragilis* toxin to maintain intestinal homeostasis and prevent lethal disease. *Cell Host Microbe.* 2017;22:443-448.e5. DOI PubMed PMC

Disclaimer/Publisher's Note: All statements, opinions, and data contained in this publication are solely those of the individual author(s) and contributor(s) and do not necessarily reflect those of OAE and/or the editor(s). OAE and/or the editor(s) disclaim any responsibility for harm to persons or property resulting from the use of any ideas, methods, instructions, or products mentioned in the content.



© The Author(s) 2026. Open Access This article is licensed under a Creative Commons Attribution 4.0 International License (https://creativecommons.org/licenses/by/4.0/), which permits unrestricted use, sharing, adaptation, distribution and reproduction in any medium or format, for any purpose, even commercially, as long as you give appropriate credit to the original author(s) and the source, provide a link to the Creative Commons license, and indicate if changes were made.